Advances in Geo-Energy Research

Vol. 13, No. 3, p. 218-230, 2024

Original article

Pore evolution modeling in natural lacustrine shale influenced by mineral composition: Implications for shale oil exploration and CO_2 storage

Liu Wang[1,2], Bo Liu[1]*, Longhui Bai[1], Zhichao Yu[3], Qiuli Huo[4], Yifei Gao[1,2]

[1]*Sanya Offshore Oil & Gas Research Institute, Northeast Petroleum University, Sanya 572025, P. R. China*

[2]*National Key Laboratory of Continental Shale Oil, Northeast Petroleum University, Daqing 163318, P. R. China*

[3]*PetroChina Exploration and Development Research Institute, Beijing 100083, P. R. China*

[4]*Daqing Oilfield Company of CNPC, Daqing 163000, P. R. China*

Keywords:
Pore evolution
natural lacustrine shale
mineral composition
CO_2 storage
Songliao Basin

Cited as:
Wang, L., Liu, B., Bai, L., Yu, Z., Huo, Q., Gao, Y. Pore evolution modeling in natural lacustrine shale influenced by mineral composition: Implications for shale oil exploration and CO_2 storage. Advances in Geo-Energy Research, 2024, 13(3): 218-230.
https://doi.org/10.46690/ager.2024.09.07

Abstract:
Describing the organic-inorganic pore evolution influenced by mineral composition is crucial for characterizing shale oil storage capacity and flow in shale, and it also helps predict storage capacity for sequestered CO_2. Using laboratory pyrolysis experiments to artificially mature shale samples at relatively high temperatures and short times, this study compares a series of natural samples with different thermal maturations, which can better reflect the real underground pore evolution. A total of 30 natural shales spanning from low to high maturity were collected from the Cretaceous Qingshankou Formation of the Songliao Basin, and the analysis results revealed four main typical shales, namely argillaceous shale, felsic shale, calcareous shale, and mixed shale. The existence of clay minerals, quartz and feldspar promote the development of $>$ 50 nm pores, while 0-20 nm pores are mainly developed in clay minerals and organic matter. When the content of total organic carbon is less than 2.5 wt.%, it displays a positive correlation with the specific surface area, but the correlation becomes negative for samples with a content of total organic carbon greater than 2.5 wt.%. The organic pores are most developed at the peak oil maturity, while inorganic pores are most developed during the oil window, and tend to be stable at high maturity. Argillaceous shale in the high maturity stage may be favorable for petroleum exploration in the Qingshankou Formation of the Songliao Basin. Mixed shale and calcareous shale may not be conducive to the short-term storage of CO_2 due to strong reactions with CO_2 at the beginning. On the other hand, argillaceous shale and felsic shale may be conducive to the long-term storage of CO_2.

1. Introduction

Shale oil and gas reservoirs are regarded not only as important replacement areas for conventional oil and gas resources but also as a favorable target layer for CO_2 storage (Wang et al., 2011; McGlade et al., 2013; Taylor and Macquaker, 2014; Zhang et al., 2023a). Interconnected organic-inorganic pore networks play a key role in the reservoir storage space and permeability in shale formations (Katz and Arango, 2018). It is crucial to understand the pore structure characteristics of shale reservoirs and the organic-inorganic pore evolution during thermal maturation (Bernard et al., 2012; Mastalerz et al., 2013; Medina et al., 2017; Wen et al., 2024).

Shale pore structure is influenced by a complex process involving various effects (Slatt and O'Brien, 2011; Liu et

Yandy Scientific Press

*Corresponding author.
E-mail address: wangliu_nepu@163.com (L. Wang); liubo@nepu.edu.cn (B. Liu); bailonghui0302@163.com (L. Bai); yuzhichao@petrochina.com.cn (Z. Yu); huoql@petrochina.com.cn (Q. Huo); gaoyifei1999@outlook.com (Y. Gao).

Received June 27, 2024; revised July 19, 2024; accepted August 13, 2024; available online August 18, 2024.

al., 2017a; Li et al., 2021). Differences in mineral composition lead to the various types of dominant reservoir space, while the main controlling factors and pore evolution models with shales of different mineral compositions will be different (Milliken, 2014; Iqbal et al., 2021). The study of Devonian Horn River shale showed that massive mudstones and pyritic mudstones with high total organic carbon (TOC) content have the highest porosity, whereas bioturbated mudstones and carbonates with low TOC content exhibit the lowest porosity (Dong et al., 2015). Based on the sample source, pore evolution has been investigated by either observing natural shale samples with different thermal maturities or conducting thermal simulation experiments on low maturity shale samples (Li et al., 2023; Xiao et al., 2024). Ko et al. (2016) collected low maturity Boquillas Formation shale samples using gold tubes under confining pressure to investigate the evolution of organic matter (OM) pores and mineral pores. The results showed that modified mineral pores account for the largest percentage during the oil generation stage, suggesting that the migration of OM and oil controls the inorganic pore network. Different from natural samples, the effect of compaction on porosity cannot be accurately evaluated during thermal simulation (Guo et al., 2017; Liu et al., 2019). In addition, short-time thermal simulation in the laboratory cannot reveal the mineral cementation and chemical transformation processes in the actual geological process, thus neglecting the influence of diagenesis on pore evolution (Tang et al., 2015; Ko et al., 2018; Liu et al., 2023c). Meanwhile, natural samples are more precious, and it is difficult to obtain a series of shale samples with different thermal maturities. Previous studies primarily focused on pore development during thermal maturation and its influencing factors (He et al., 2022; Liu et al., 2022a; Wang et al., 2023). For the Longmaxi shale in the Sichuan basin, the total porosity decreases rapidly due to compaction when vitrinite reflectance (R_o) is less than 0.7% and increases due to hydrocarbon generation and dissolution when R_o is 0.7%-1.3% (Liu et al., 2017b). For the Devonian Duvernay Formation in Canada, the total volume decreases greatly due to compaction when R_o is less than 0.5% and increases slightly due to primary cracking of OM when R_o is 0.55%-0.65%. The decrease occurs because of oil filling and bitumen formation when R_o is 0.65%-1.15% and the increase is because of the secondary cracking of OM when R_o is more than 1.15% (Dong et al., 2019). Therefore, inorganic and organic factors simultaneously control the shale pore evolution process, which complicates the understanding of shale pore structure evolution. Furthermore, the differences in the evolution of organic and inorganic pores are still unclear.

The Songliao Basin is one of the largest continental petroleum-bearing basins in the world (Bai et al., 2022; Liu et al., 2023a), which provides excellent natural samples with different evolution stages and mineral compositions for studying the evolution and controlling factors of various genetic pores in shale. In addition, a large amount of inorganic CO_2 has been discovered in the Songliao Basin. Complex diagenesis occurred between CO_2 and shale under long geological time and low geothermal temperature conditions, which can provide a reference for the study of the diagenetic effects of CO_2 on shale sealing after long-term storage (Hou et al., 2022). Accordingly, the main objectives of this paper are to:

1) Analyze the main controlling factors of pore structure parameters in shales with various mineral compositions.
2) Establish an organic-inorganic pore evolution model.
3) Identify the favorable shale targets of petroleum exploration and CO_2 storage.

This work enhances our understanding of the complex control exerted by various factors on organic-inorganic pore evolution, promoting the exploration of shale oil and sequestered CO_2 in the studied area.

2. Sample and methods

A total of 30 core samples were collected from 8 wells. The mineral compositions, geochemical parameters and microstructure were identified by X-Ray Diffraction, TOC content, R_o and thin section observation. The pore morphology and diagenetic types were determined by field emission scanning electron microscope (FE-SEM). Automatic shale organic and inorganic porosity quantification were obtained the by edge-threshold automatic processing (ETAP) technique (Tian et al., 2021). Pore structure characterization was done by low temperature nitrogen adsorption (LN_2A) and mercury intrusion capillary pressure (MICP). The location of 8 wells in the Songliao Basin is shown in Fig. S1 of the supporting information, which section also includes the description of specific procedures of all experimental methods.

3. Results

3.1 Mineralogy and geochemical characteristics

According to the mineral composition and thin section observations, four kinds of shale samples can be recognized (Fig. 1): Argillaceous shale, felsic shale, mixed shale, and calcareous shale. The average TOC content in the order of high to low is: Argillaceous shale (avg. 2.75 wt.%), felsic shale (avg. 2.66 wt.%), mixed shale (avg. 2.24 wt.%), and calcareous shale (avg. 1.98 wt.%). The R_o value ranges from 0.6% to 1.67%, covering a low mature-high mature stage. The details of mineralogical compositions and organic geochemical data of shale samples for the Qingshankou Formation can be found in Table S1 of the supporting information.

3.2 Porosity data from FE-SEM

3.2.1 Pore types

(1) Inorganic pores

Inorganic pores mainly include interparticle pores, intercrystalline pores and intraparticle pores. Interparticle pores in the Qingshankou Formation generally develop in brittle minerals and clay mineral. The pore shapes are triangular and elongated, and the pore diameter ranges from 10 to 100 nm (Figs. 2(a)-2(b)). Intercrystalline pores in the Qingshankou Formation are found in pyrite and clay minerals. The pore diameter is between 40 and 100 nm (Figs. 2(c)-2(e)). Intraparticle pores develop inside particles and include primary pores and dissolution pores formed during the oil window.

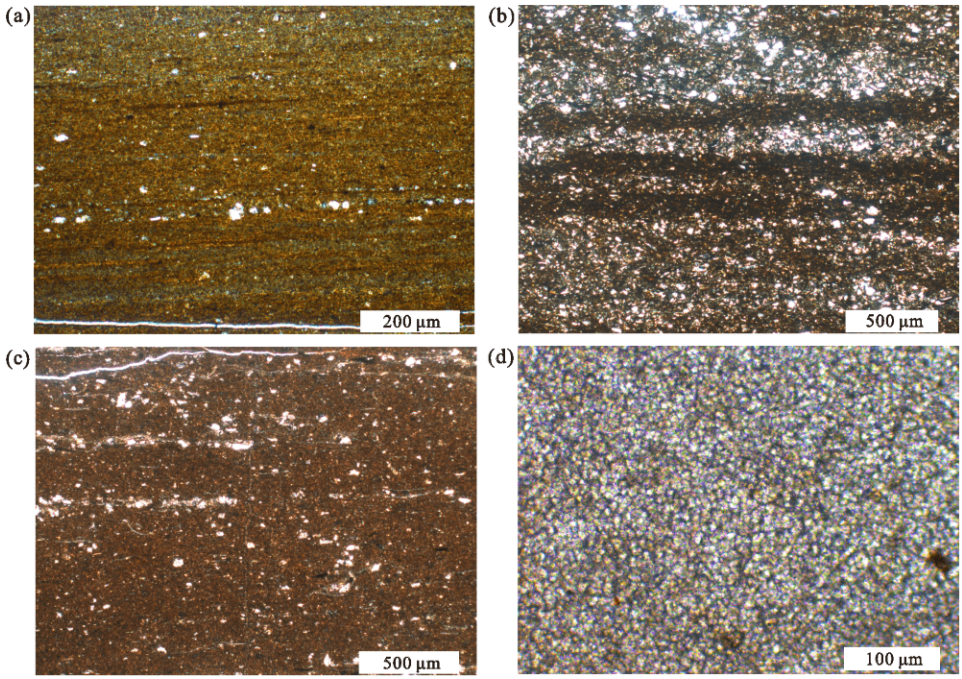

Fig. 1. Identification of different shale lithofacies by thin section. (a) Argillaceous shale (A544-01, single polarized light), (b) felsic shale (A36-02, single polarized light), (c) mixed shale (A3-01, single polarized light) and (d) calcareous shale (A68-01, single polarized light).

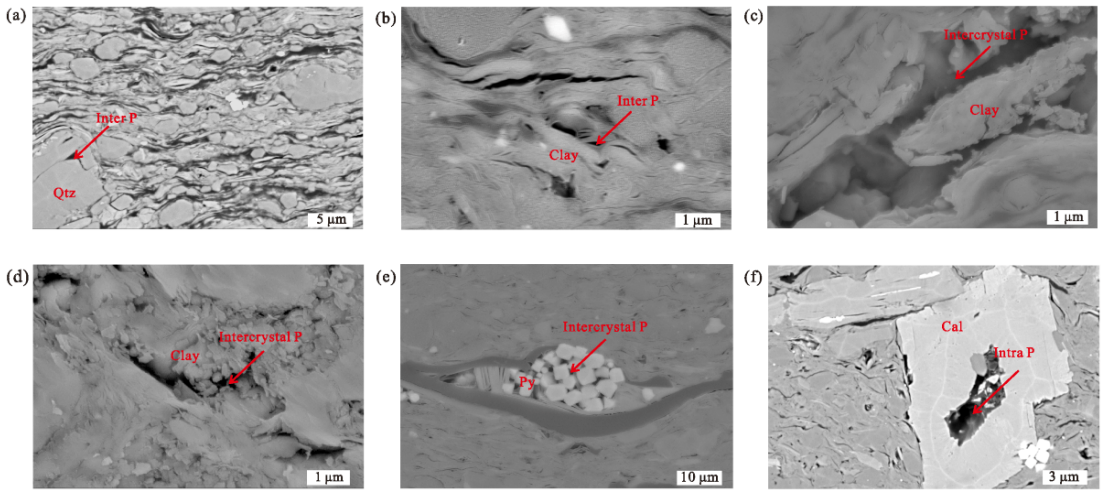

Fig. 2. FE-SEM images of inorganic pores. (a) Interparticle pores between quartz particle, A68-02, (b) clay mineral interparticle pores, A17-03, (c) clay mineral intercrystal pores, A544-01, (d) clay mineral intercrystal pores, A3-05, (e) pyrite intercrystal pores, A3-05 and (f) intraparticle pores in Calcite, A58-02. Qtz: Quartz, Inter P: Interparticle pores, Intercrystal P: Intercrystal pores, Py: Pyrite, Intra P: Intraparticle pores, Cal: Calcite.

Primary intraparticle pores are rarely found in the Qingshankou Formation. Dissolved pores are developed inside the K-feldspar and calcite mineral in the oil generation window. The shape of the dissolved pores is oval or irregular harbor-shaped, and the pore diameter ranges from 100 nm to 2 μm (Fig. 2(f)).

(2) Organic pores

The low maturity stage is characterized by the development of few primary OM pores. At the beginning of the early oil generation stage, OM-mineral pores are observed, which are partly or fully lined with migrated OM (Fig. 3(a)). At the peak oil generation, a large number of bubble-like pores formed by gas release develop on OM with a pore diameter of less than 20 nm (Fig. 3(b)). Spongy pores comprise the main OM pore type in the high maturity stage (Figs. 3(c) and 4(d)). For more details about organic pores development, readers can refer to recent literatures (e.g., Wang et al., 2023).

(3) Cracks

Cracks in the Qingshankou formation of the Songliao Basin can be divided into organic cracks and inorganic cracks.

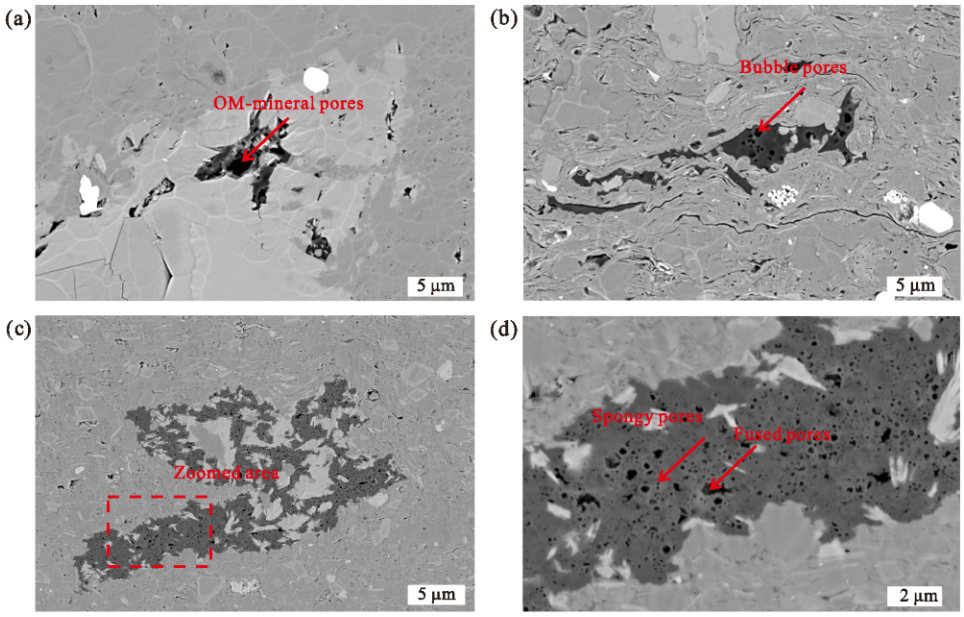

Fig. 3. FE-SEM images of organic pores. (a) OM-mineral pores, A21-03, (b) bubble pores, A17-01, (c) spongy pores, where the red square indicates the zoomed area, A1-07 and (d) the area indicated by the red rectangle in (c), A1-07.

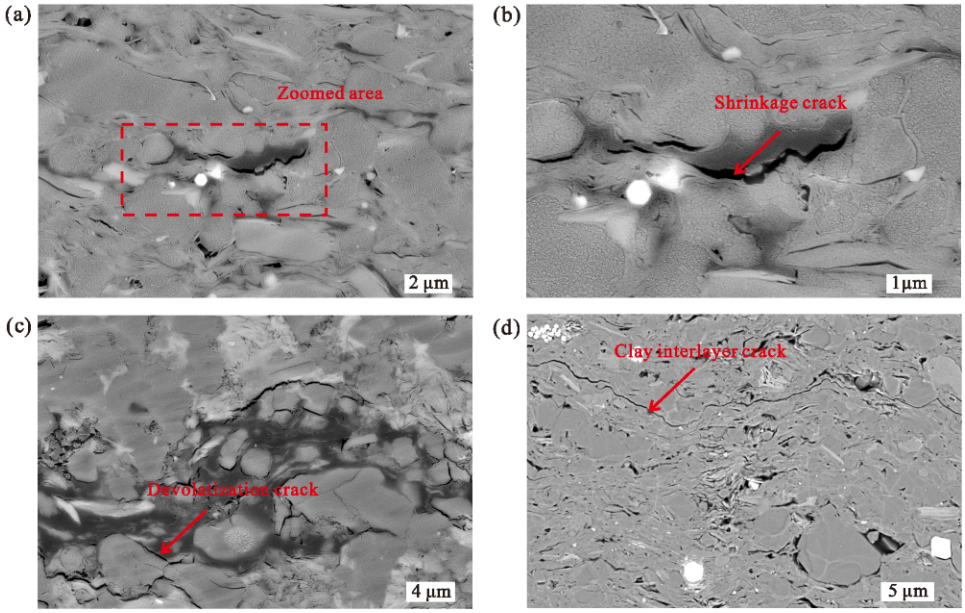

Fig. 4. (a) Shrinkage crack, where the red square indicates the zoomed area, A21-04, (b) the area indicated by the red rectangle in (a), (c) devolatilization crack, A58-01 and (d) clay interlayer crack, A1-07.

Organic cracks can be classed into OM shrinkage cracks and devolatization cracks. OM shrinkage cracks are the result of the volume shrinkage of OM after hydrocarbon generation and cracks formed within the OM or at the contact surface with other minerals (Figs. 4(a)-4(b)). Devolatilization cracks are formed due to the degassing or pressure release of solid bitumen (Fig. 4(c)). Inorganic cracks refer to clay interlayer cracks, generally developed along the bedding and exhibiting a length of several μm and a width of 10-100 nm (Fig. 4(d)). The clay interlayer cracks connect the inorganic and organic pores and become the lateral migration channels of oil and gas in the reservoir.

3.2.2 Automatic porosity quantificatio

In argillaceous shale, the average content of intercrystal pores is the highest (22%), followed by interparticle pores, inorganic cracks and OM pores, at 21%, 19% and 17%, respectively (Fig. 5). The average total surface porosity is 0.687%, and the average organic porosity and inorganic porosity are 0.127% and 0.560% respectively (Fig. 6). In felsic shale, the content of inorganic pores is the highest (69%), followed by intercrystal pores, interparticle pores and intraparticle pores

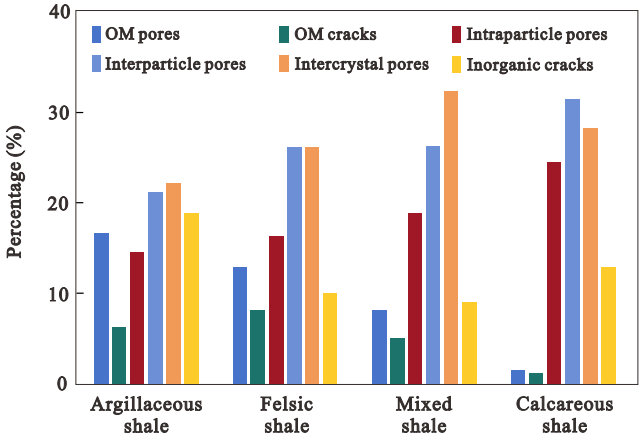

Fig. 5. SEM-based average percentage of various pores and cracks via ETAP.

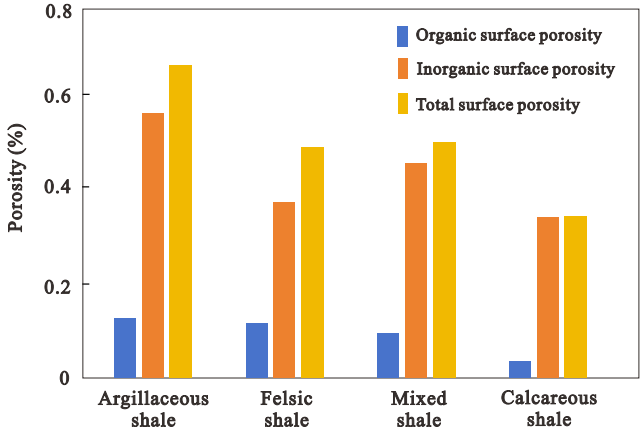

Fig. 6. Average organic surface porosity, inorganic surface porosity and total surface porosity of shale samples of the Qingshankou Formation in the Songliao Basin.

with 26%, 26% and 16%, respectively, then by OM pores and inorganic cracks with 13% and 10%, respectively (Fig. 5). The average total surface porosity is 0.484%, and the average organic porosity and inorganic porosity are 0.114% and 0.371%, respectively (Fig. 6). In mixed shale, the average content of inorganic pores is also the highest (78%), followed by intercrystal pores, interparticle pores and intraparticle pores, with 33%, 26% and 19%, respectively, then by inorganic cracks and OM pores, with 9% and 8%, respectively (Fig. 5), The average total surface porosity is 0.498%, and the average organic porosity and inorganic porosity are 0.094% and 0.454%, respectively (Fig. 6). In calcareous shale, OM pores are rare (1%). Intercrystal pores, intraparticle pores, interparticle pores, and inorganic cracks constitute 28%, 32%, 19% and 9% of the total pore space, respectively (Fig. 5). The average total surface porosity is 0.342%, and the average organic porosity and inorganic porosity are 0.036% and 0.339%, respectively (Fig. 6). The percentage details of different pore types of shale samples obtained from automatic porosity quantification can be found in Table S2 of the supporting information.

3.3 Pore structure characterization

3.3.1 Analysis of LN_2A

(1) Pore structure parameter from LN_2A

The maximum adsorption capacity of the Qingshankou Formation is between 0.88095-3.05341 cm^3/g, with an average of 1.9544 cm^3/g. The average maximum adsorption capacity of different shale types from high to low is determined as argillaceous shale, felsic shale, mixed shale and calcareous shale (Fig. 7(a)). The specific surface area (SSA) of shales in the Qingshankou Formation is distributed between 6.2577-33.1692 m^2/g, with an average SSA of 19.5922 m^2/g (Fig. 7(b)). The pore volume distribution is between 0.030704-0.106647 cm^3/g, and the average pore volume is 0.060766 cm^3/g (Fig. 7(c)). The average pore diameter is between 6.97-20.80 nm, with an average of 12.90 nm (Fig. 7(d)).

A positive correlation is established between SSA and pore volume, and an obvious negative correlation is found between the SSA and average pore diameter (Fig. 8). The average SSA and pore volume from high to low is: Argillaceous shale, mixed shale, felsic shale, and calcareous shale. The average pore diameter shows the opposite trend to SSA and pore volume.

3.3.2 Pore size distribution of LN_2A and MICP

The combination of LN_2A and MICP can be used to detect pores ranging from micro- to macroscale. The lower detection limit of gas adsorption method is 0.35 nm, and the upper detection limit of MICP is 1 mm (Sun et al., 2024). The former can effectively reflect the distribution of nanopores in shale, while the latter can reflect information about shale macropores and microcracks (Chalmers and Bustin, 2008). Therefore, this study uses LN_2A to characterize pores sized less than 50 nm and MICP to characterize pores sized greater than 50 nm, and subdivides pores sized less than 50 nm into those in the 0-20 and 20-50 nm size ranges.

In general, pores smaller than 50 nm provide most of the pore volume of the Qingshankou Formation shale. When the pore size is less than 50 nm, the pore volume shows an asymmetric bimodal distribution, with peaks located between 7-18 and 30-37 nm, respectively. The curve envelope area in the range of 7-18 nm is significantly higher than that of 30-37 nm (Fig. 9). When the pore size is greater than 50 nm, microcracks develop in argillaceous shale and mixed shale and the peak pore size is greater than 104 nm (Figs. 9(a) and 9(c)). In the range of 100-104 nm, the pore size of felsic shale and calcareous shale present multimodal distribution. In the A58-01 and A21-01 samples, the pore volume shows a downward trend in the space greater than 104 nm. Considering the influence of "blank effect", the error of experimental results for pore sizes larger than 10,000 nm is relatively high (Sun et al., 2024).

4. Discussion

4.1 Factors controlling pore development

During shale deposition and diagenesis, the pore structure is controlled by multiple factors at different stages (Milliken et al., 2013; Dong et al., 2019; Gao et al., 2020; Liu et al., 2023b), such as maturity, type of macerals and diagenesis (Fauchille et al., 2017; Dowey and Taylor, 2020; Liu et

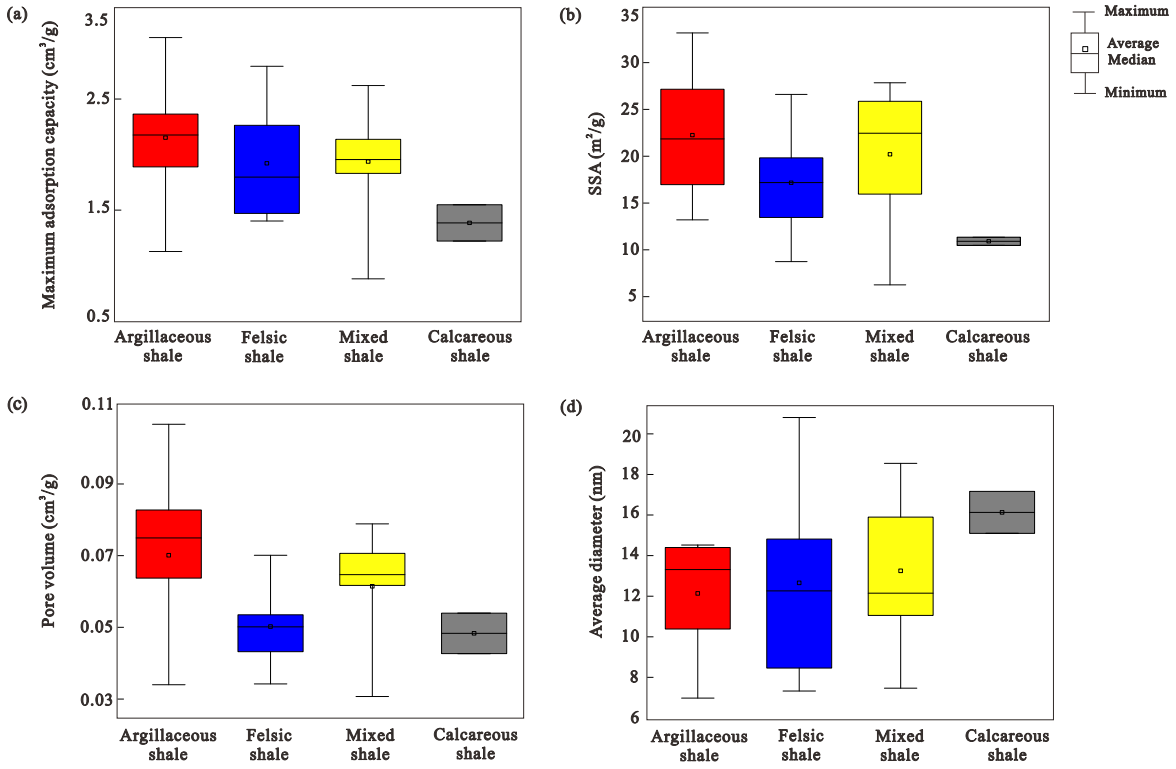

Fig. 7. Maximum adsorption capacity, SSA, pore volume, and average diameter range of different lithofacies in the Qingshankou shale of the northern Songliao Basin. (a) Argillaceous shale, (b) felsic shale, (c) mixed shale and (d) calcareous shale.

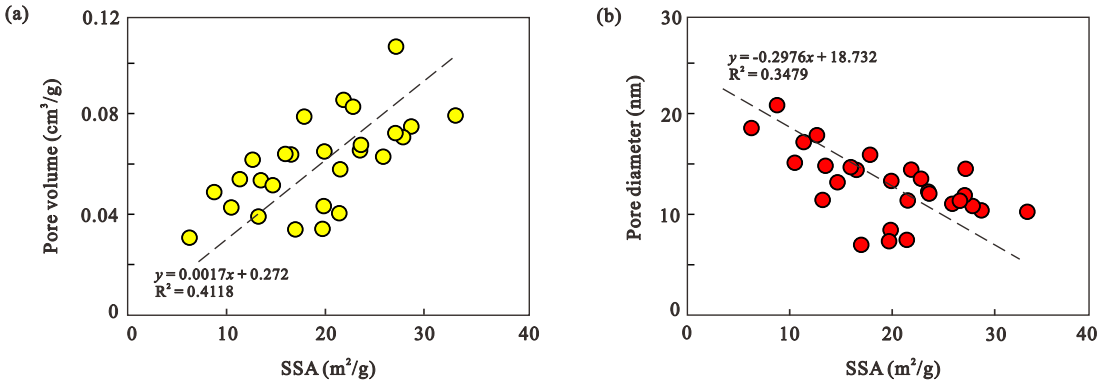

Fig. 8. Correlations between (a) SSA and pore volume and (b) SSA and pore diameter of the Qingshankou Formation in the Songliao Basin.

al., 2022a). This study focused on the influence of mineral composition and TOC content on pore evolution with respect to 0-20, 20-50 and > 50 nm sized shale pores. Since the pore size of organic pores observed under SEM is mostly less than 20 nm, to better determine the correlation between organic pores and mineral composition, pores smaller than 50 nm were further divided into 0-20 and 20-50 nm pores.

4.1.1 Mineral composition

(1) Clay minerals

The SSA is in direct proportion to the clay mineral content for argillaceous shale, but this is not obvious for other shale samples (Fig. 10(a)). Since the SSA is also in direct proportion to the pore volume but in inverse proportion to the average pore size (Fig. 8), it can be inferred that the clay mineral content for argillaceous shale increases with the pore volume and decreases with the average pore size. This might be attributed to the layered crystal structure and the small distance (~nanometers) between crystal planes for clay minerals (Ross and Bustin, 2009). Therefore, shale with high clay mineral content has a high SSA, which can provide a large number of pore spaces. Clay minerals promote the development of 0-20 and > 50 nm pores in shale samples, whereas they contribute less to 20-50 nm pores (Fig. 10(d)). The clay minerals in the Qingshankou Formation of the Songliao Basin mainly contain illite/smectite mixed layer and illite, with minor chlorite/smectite mixed layer and chlorite (He et al., 2022). At the low maturity stage, macropores and

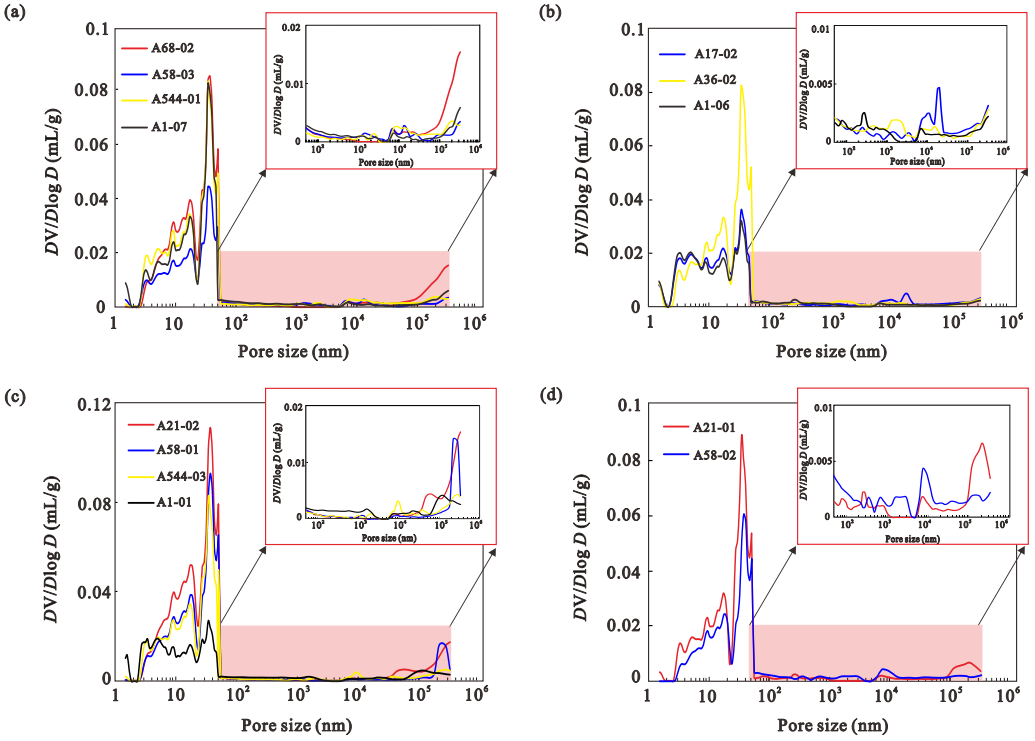

Fig. 9. *DV*/*D*log*D* vs pore width of the Qingshankou Formation in the Songliao Basin based on LN_2A and MICP. (a) Argillaceous shale, (b) felsic shale, (c) mixed shale and (d) calcareous shale. Pore sizes less than 50 nm are characterized by LN_2A, while pore sizes greater than 50 nm are characterized by MICP.

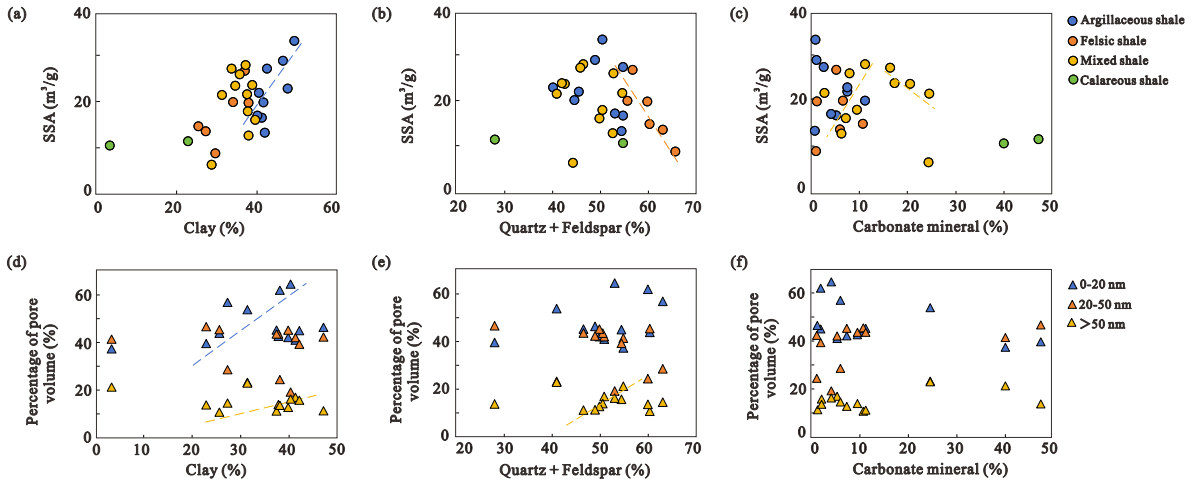

Fig. 10. Correlations between (a) SSA and clay content, (b) SSA and quartz + feldspar content, (c) SSA and carbonate mineral content, (d) percentage of pore volume and clay content, (e) percentage of pore volume and quartz + feldspar content and (f) percentage of pore volume and carbonate mineral content of the Qingshankou Formation in the Songliao Basin.

mesopores between smectite aggregates decrease with increasing compaction, while micropores are almost unaffected (Kuila and Prasad, 2010). As the maturity increases, the smectite in the illite/smectite mixed layer and chlorite/smectite mixed layer will gradually transform into illite and chlorite. This process releases interlayer water, leading to interlayer collapse. In addition, the volume of clay mineral particles shrinks to form intercrystal pores and interlayer cracks (Figs. 2(c)-2(d) and 4(d)), resulting in the development of 0-20 and $>$ 50 nm pores. A previous study observed more abundant organic pores in organic-clay mixtures rather than single OM in the Songliao Basin, which indicates that the clay mineral promotes the generation of OM hydrocarbon (Cai et al., 2022; Chang et al., 2022). The size of organic pores in organic-clay mixtures is usually less than 20 nm, which further explains why 0-20 nm pores are preserved in shale samples with high clay content.

(2) Quartz and feldspar

The content of quartz + feldspar is in inverse proportion

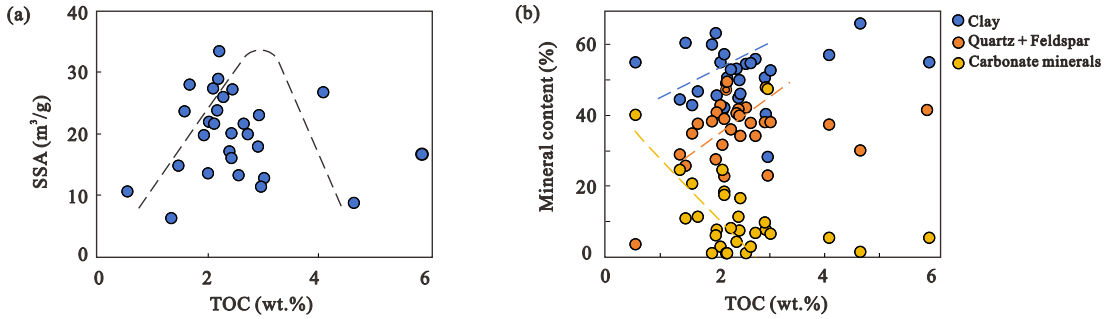

Fig. 11. Correlations between (a) TOC and SSA and (b) TOC and mineral content of the Qingshankou Formation in the Songliao Basin.

to the SSA and pore volume but in direct proportion to the average pore size for felsic shale (Fig. 10(b)). Moreover, the content of quartz + feldspar mainly has a weak positive correlation with pores larger than 50 nm and no obvious correlation with those sized 0-20 and 20-50 nm (Fig. 10(e)), consistent with previous studies in the Western Canada Basin (Ross and Bustin, 2009; Dong et al., 2019). This finding indicates that > 50 nm pores are mainly developed on feldspar and quartz minerals. One possible explanation is that the mechanical compaction dominates in the early diagenetic stage, and skeleton-support siliceous minerals can provide a rigid framework that prevents the collapse of clay platelets (Liu et al., 2022b). Part of the intergranular pores are retained under the support of quartz or feldspar, which have larger pore sizes (Fig. 2(a)). Furthermore, the pore size of dissolved pores developed in feldspar grains is generally several microns in the early oil maturity stage (Fig. 3(a)).

(3) Carbonate minerals

Carbonate minerals are more abundant in calcareous shale and mixed shale, but the correlation between carbonate mineral content and pore structure parameter is not obvious (Figs. 10(c) and 10(f)). The potential explanation could be that carbonate minerals mainly develop harbor-shaped and large-size dissolution pores at the early maturity stage (Fig. 2(f)). After peak oil maturity, calcite cementation and the migration of OM will block these pores (Zhang et al., 2023b), so pores with different sizes develop in carbonate minerals.

4.1.2 TOC content

TOC has an important impact on the development of shale reservoir pores, especially organic pores (Milliken et al., 2013; Löhr et al., 2015). Fig. 11(a) shows that SSA increases and then decreases with a TOC threshold of 2.5 wt.%. The possible reason might be that due to lower shale permeability, hydrocarbons formed during the oil window cannot discharge from the shale reservoir in time, thus reducing the SSA (Ohiara et al., 2024). It is found that TOC increases with the content of clay minerals, quartz and feldspar (Fig. 11(b)). The possible explanations include:

1) The SSA of clay minerals is significantly larger than that of other minerals, so the adsorption capacity of OM is also the strongest (Cai et al., 2022). The organic-clay complex is a special mixture in the Qingshankou Formation. The organic-clay mixtures developed more organic pores than single OM (Figs. 3(b)-3(c)), which is attributed to the fact that clay minerals can significantly catalyze the OM hydrocarbon generation (Wang et al., 2023).
2) Feldspar and quartz also have a supporting effect on organic pores (Emmings et al., 2020).

By contrast, TOC decreases with carbonate content (Fig. 11(b)), for the likely reason that calcite cementation can block organic pores (Ohiara et al., 2024). The results of average TOC content and organic porosity in shale samples also validate these statements. The TOC content and organic surface porosity for argillaceous shale are the highest, followed by felsic shale, and they are the lowest in calcareous shale (Table S1, Fig. 5).

4.2 Porosity evolution model

4.2.1 Pore evolution of shales with different mineral compositions

At the low maturity stage, pore evolution in argillaceous shale is dominated by compaction. The clay minerals are directionally distributed, and OM is also squeezed and deformed and often complexed with clay minerals (Figs. 2(a) and 12(a)). This is related to the algae accumulation caused by the flocculation of clay (Theng, 1971; Stasiuk, 1993; Wang et al., 2022). Organic pores and cracks are less developed, accounting for 5% and 8% of the total number of pores, respectively. The intergranular and intercrystalline pores of clay minerals are more developed, which account for 49% of the total number of pores (Table S2). At the early oil maturity stage, the impact of compaction on the reservoir space gradually weakens. OM begins to generate hydrocarbons, followed by the formation of shrinkage cracks (Figs. 3(b), 4(a)-4(b) and 12(b)). At the peak oil maturity stage, as the degree of clay mineral transformation increases, the intercrystalline pores and interlayer cracks within clay minerals further develop, accounting for 25% and 18% of the total number of pores, respectively (Table S2). However, when it comes to the late oil maturity stage, migrated OM fills the pores and the mineral matrix (Fig. 12(c)), and the proportion of OM pores and cracks significantly decrease. At the high maturity stage, OM will be further converted into pyrobitumen and gas (Liu et al., 2022a), accompanied by the formation of spongy pores (Fig. 12(d)). The content of organic pores increases to 20%

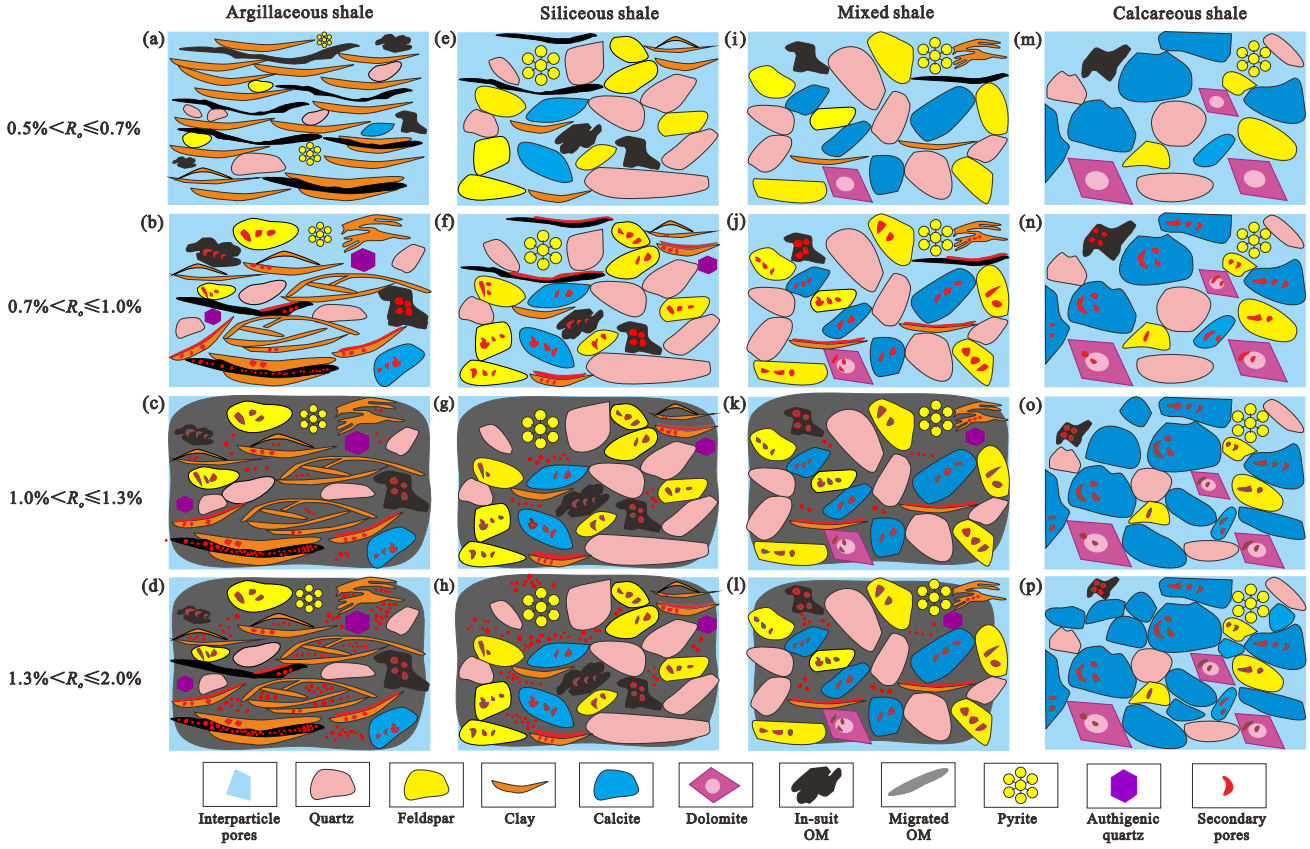

Fig. 12. Conceptual model of pore evolution for various typical shale samples.

and the proportion of inorganic pores does not change much (Table S2). Felsic shale with high detrital mineral content shows weaker compaction than that of argillaceous shale at the low maturity stage. Part of the intergranular pores and organic pores are retained by the support of rigid minerals. Organic pores and intergranular pores occupy 10% and 29% of the total pore content, respectively (Table S2). From the early maturity stage, the organic acids formed during the oil window begin to dissolve K-feldspar in felsic shale (Figs. 12(e)-12(h)). Similar to felsic shale, mixed shale at the low maturity stage has stronger resistance to compaction than argillaceous shale. The dissolved mineral in the oil window is feldspar and calcite, and intragranular pores account for 17% (Figs. 12(i)-12(l)). At the late oil maturity stage, the migrated OM charged in pores. In addition, as the organic acid is consumed, the formation fluid gradually transforms into alkaline, combines with the solution carrying Ca^{2+} to form calcite, then blocks pores through calcite cementation (Tissot and Welte, 1984; Zhang, 2018). Among the four types of shale samples, calcareous shale has the lowest total surface porosity (Table S2). Organic pores and cracks are hardly developed during the thermal maturation, and there is also little migrated OM to fill the pores in the late oil maturity stage, which is related to the low TOC content in calcareous shale. The dissolved mineral in the oil window is dolomite and calcite. In the late oil maturity stage, carbonate cementation is very obvious (Fig. 12(m)-12(p)).

4.2.2 Organic-inorganic pore evolution model

The Qingshankou Formation is divided into 3 maturity stages: Low maturity ($0.5\% < R_o \leq 0.7\%$), mature ($0.7\% < R_o \leq 1.3\%$), and high maturity ($1.3\% < R_o \leq 2.0\%$). The mature stage is further subdivided into: Early oil mature ($0.7\% < R_o < 1.0\%$), peak oil mature ($R_o = 1.0\%$) and late oil mature ($1.0\% < R_o \leq 1.3\%$). Based on the above research, we propose a dual-pore evolution model of the Qingshankou shale, which is mainly divided into four stages (Fig. 13).

1) At the low maturity stage ($0.5\% < R_o \leq 0.7\%$), the total surface porosity shows a downward trend. The primary pore is lost in large quantities under compaction, which is more obvious in argillaceous shale (Figs. 13(a)). The ratio of OM pores decreases rapidly and only a few intergranular pores with large pore size develop. As a consequence, the average pore size increases slightly while the pore volume and SSA reduce.
2) From early to the peak oil maturity ($0.7\% < R_o \leq 1.0\%$), the total surface porosity begins to show an increasing trend and reaches the first secondary pore development zone at the peak oil maturity. The ratio of inorganic pores increases when R_o is 0.84% due to dissolution and clay mineral transformation (Fig. 13(b)), and the ratio of OM pores increases due to the formation of bubble pores during thermal maturation. Since the organic pores produced at this stage have relatively small pore sizes, the average pore size decreases slightly and the pore volume

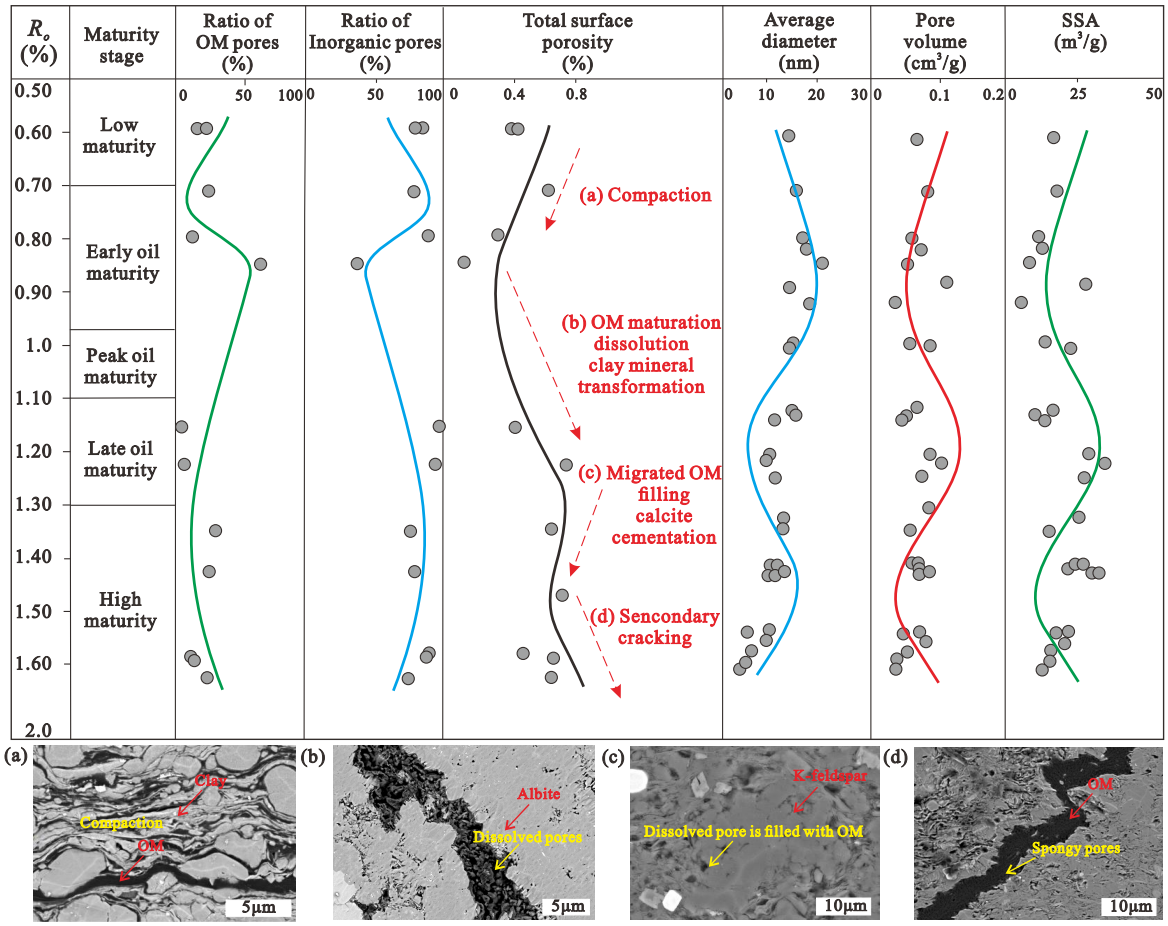

Fig. 13. Organic-inorganic pore evolution model. (a) A68-02, (b) A21-04, (c) A36-02 and (d) A3-05.

and SSA increase.

3) In the late oil maturity stage ($1.0\% < R_o \leq 1.3\%$), the total surface porosity shows a downward trend due to the migrated OM occupies the secondary pore spaces, while the cementation developed in mixed shale and calcareous shale will also block pores (Fig. 13(c)). The hydrocarbon generation of OM is weakened compared with the peak oil maturity, so the ratio of OM pores decreases. The remaining pores have large sizes, so the average pore diameter increases slightly and the pore volume and SSA show a downward trend.
4) In the high maturity stage ($1.3\% < R_o \leq 2.0\%$), the total surface porosity shows an upward trend. The compressive resistance and stability of the rock skeleton are greatly improved and the inorganic porosity is relatively stable. The secondary cracking of oil and post-oil bitumen at the high maturity stage produces spongy pores (Fig. 13(d)), and the total surface porosity increase significantly. The average pore diameter is decreased, and the pore volume and SSA are both increased.

4.3 Implications for favorable petroleum exploration and CO_2 storage

Our study above demonstrated that thermal maturity, TOC and mineral composition are the main controlling factors of pore evolution in the Qingshankou Formation of the Songliao Basin. The content of clay minerals in argillaceous shale is relatively high and it has a strong correlation with pore volume (Figs. 10(a)-10(d)). The organic-clay complex lays the foundation for later OM hydrocarbon generation, while argillaceous shale has the highest average TOC value at 2.75 wt.%. Combined with the extensive distribution of argillaceous shale in the Qingshankou formation (Liu et al., 2023a), the argillaceous shale in the high maturity stage could be favorable lithofacies for petroleum exploration in the Qingshankou Formation of the Songliao Basin.

Three potential reasons for the leakage of caprock include: (1) Leakage along faults and micro-fractures; (2) mechanical damage; (3) chemical dissolution (Vialle et al., 2016). As a limitation of this study, it only evaluates the CO_2 storage capacity from chemical dissolution and focuses on shale caprocks with different mineral compositions. The self-sealing effects of caprocks with different mineral compositions are different. After CO_2 is injected into the ground, it will first react with the formation water to form acidic fluids. Carbonate minerals such as calcite and dolomite are the most sensitive to these acidic fluids (Ma et al., 2021; Dávila et al., 2017; Zhou et al., 2022). The presence of dissolution pores on the calcite also indicates a reaction with CO_2, posing a leakage risk (Fig. 2(f)). However, the precipitation of new carbonate minerals

will alleviate the dissolution of carbonate minerals, reducing the reservoir porosity. In addition, the injection of CO_2 will also react with feldspars and clay minerals, but the dissolution of feldspars and clay minerals is relatively mild due to the relevant reaction rate constants with CO_2 being 7-10 orders of magnitude lower than those of carbonate minerals (Hou et al., 2022; Wang et al., 2024). Overall, it can be inferred that mixed shale and calcareous shale rich in carbonate minerals cannot be not conducive to the safe geological sequestration of CO_2 in the short term (during the injection period, i.e., over 25-50 years) due to their strong reaction with CO_2 at the beginning, while argillaceous shale and felsic shale rich in clay minerals and feldspar are be conducive to the safe geological sequestration of CO_2 in long-term storage (during the storage phase with time scales over 100 years and up to 10 kyrs).

5. Conclusion

1) Clay minerals have a positive correlation with SSA and pore volume, which can promote the development of 0-20 nm and $>$ 50 nm pores in shale. Quartz + feldspar have a negative correlation with the SSA and pore volume, which promotes the development of $>$ 50 nm pores in shale. When the TOC content is $<$ 2.5 wt.%, it has a positive correlation with the SSA; when it is $>$ 2.5 wt.%, this correlation is negative, which is related to the clogging of pores by migrating OM after the peak oil maturity.
2) The storage space of argillaceous shale is dominated by OM pores, intercrystalline pores and cracks of clay minerals. Felsic shale mainly develops organic pores, rigid mineral intergranular pores and feldspar dissolution pores. Mixed shale mainly develops clay minerals intercrystalline pores and dissolution pores. Calcareous shale mainly develops carbonate mineral dissolution pores. And OM pores are hardly developed.
3) The organic-inorganic pore evolution model can be divided into four stages. (1) In the low maturity stage, organic pores and inorganic pores are affected by compaction. It only developed a few intergranular pores. (2) In the early oil maturity stage, OM begins to generate hydrocarbons and the organic pores increase. Affected by dissolution and transformation of clay minerals, inorganic pores also begin to increase when R_o is 0.84%. (3) In the late oil maturity stage, organic pores decline due to the dual effects of OM migration and cementation filling. Inorganic pores increase due to further transformation of clay mineral. (4) At the high maturity stage, organic pores increase again, while the inorganic pores remain basically stable.
4) Argillaceous shale in the high maturity stage may be favorable for petroleum exploration in the Qingshankou Formation of the Songliao Basin. Mixed shale and calcareous shale may not beneficial to short-term storage of CO_2, while their sealing capacity can be enhanced over time due to authigenic mineral precipitation. Argillaceous shale and felsic shale are likely effective in long-term CO_2 storage.

Acknowledgements

This study was supported by the National Natural Science Foundation of China (No. U22A20574) and the Hainan Province Science and Technology Special Fund (No. ZDYF2023GXJS009).

Supplementary file

https://doi.org/10.46690/ager.2024.09.07

Conflict of interest

The authors declare no competing interest.

References

Bai, L., Liu, B., Du, Y., et al. Distribution characteristics and oil mobility thresholds in lacustrine shale reservoir: Insights from N_2 adsorption experiments on samples prior to and following hydrocarbon extraction. Petroleum Science, 2022, 19(2): 486-497.

Bernard, S., Wirth, R., Schreiber, A., et al. Formation of nanoporous pyrobitumen residues during maturation of the Barnett Shale (Fort Worth Basin). International Journal of Coal Geology, 2012, 103: 3-11.

Cai, J., Du, J., Chao, Q., et al. Evolution of surface acidity during smectite illitization: Implication for organic carbon cycle. Marine and Petroleum Geology, 2022, 138: 105537.

Chalmers, G. R. L., Bustin, R. M. Lower Cretaceous gas shales in northeastern British Columbia, Part I: Geological controls on methane sorption capacity. Bulletin of Canadian Petroleum Geology, 2008, 56(1): 1-21.

Chang, J., Fan, X., Jiang, Z., et al. Differential impact of clay minerals and organic matter on pore structure and its fractal characteristics of marine and continental shales in China. Applied Clay Science, 2022, 216: 106334.

Dávila, G., Cama, J., Luquot, L., et al. Experimental and modeling study of the interaction between a crushed marl caprock and CO_2-rich solutions under different pressure and temperature conditions. Chemical Geology, 2017, 448: 26-42.

Dong, T., Harris, N. B., Ayranci, K., et al. Porosity characteristics of the Devonian Horn River shale, Canada: Insights from lithofacies classification and shale composition. International Journal of Coal Geology, 2015, 141-142: 74-90.

Dong, T., Harris, N. B., McMillan, J. M., et al. A model for porosity evolution in shale reservoirs: An example from the Upper Devonian Duvernay Formation, Western Canada Sedimentary Basin. AAPG Bulletin, 2019, 103(5): 1017-1044.

Dowey, P. J., Taylor, K. G. Diagenetic mineral development within the upper Jurassic Haynesville-Bossier shale, USA. Sedimentology, 2020, 67(1): 47-77.

Emmings, J. F., Dowey, P. J., Taylor, K. G., et al. Origin

and implications of early diagenetic quartz in the Mississippian Bowland Shale Formation, Craven Basin, UK. Marine and Petroleum Geology, 2020, 120: 104567.

Fauchille, A. L., Ma, L., Rutter, E., et al. An enhanced understanding of the Basinal Bowland shale in Lancashire (UK), through microtextural and mineralogical observations. Marine and Petroleum Geology, 2017, 86: 1374-1390.

Gao, Z., Fan, Y., Xuan, Q., et al. A review of shale pore structure evolution characteristics with increasing thermal maturities. Advances in Geo-Energy Research, 2020, 4(3): 247-259.

Guo, H., Jia, W., Peng, P., et al. Evolution of organic matter and nanometer-scale pores in an artificially matured shale undergoing two distinct types of pyrolysis: A study of the Yanchang Shale with Type II kerogen. Organic Geochemistry, 2017, 105: 56-66.

He, W., Liu, B., Sun, M., et al. Pore types, genesis, and evolution model of lacustrine oil-prone shale: A case study of the Cretaceous Qingshankou Formation, Songliao Basin, NE China. Scientific Reports, 2022, 12(1): 17210.

Hou, L., Yu, Z., Luo, X., et al. Self-sealing of caprocks during CO_2 geological sequestration. Energy, 2022, 252: 124064.

Iqbal, M. A., Rezaee, R., Smith, G., et al. Shale lithofacies controls on porosity and pore structure: An example from Ordovician Goldwyer Formation, Canning Basin, Western Australia. Journal of Natural Gas Science and Engineering, 2021, 89: 103888.

Katz, B. J., Arango, I. Organic porosity: A geochemist's view of the current state of understanding. Organic Geochemistry, 2018, 123: 1-16.

Ko, L. T., Loucks, R. G., Zhang, T., et al. Pore and pore network evolution of Upper Cretaceous Boquillas (Eagle Ford-equivalent) mudrocks: Results from gold tube pyrolysis experiments. AAPG Bulletin, 2016, 100(11): 1693-1722.

Ko, L. T., Ruppel, S. C., Loucks, R. G., et al. Pore-types and pore-network evolution in Upper Devonian-Lower Mississippian Woodford and Mississippian Barnett mudstones: Insights from laboratory thermal maturation and organic petrology. International Journal of Coal Geology, 2018, 190: 3-28.

Kuila, U., Prasad, M. Pore size distribution and ultrasonic velocities of compacted Na-montmorillonite clays. SEG Technical Program Expanded Abstracts, 2010, 2590-2594.

Li, P., Zhou, S., Liu, Q., et al. Mechanism of water-induced alterations to nanoscale pores: Implications from anhydrous versus hydrous pyrolysis. Fundamental Research, 2023, https://doi.org/10.1016/j.fmre.2023.07.014. (in Press)

Liu, B., Liu, L., Fu, J., et al. The Songliao super basin in northeastern China. AAPG Bulletin, 2023a, 107(8): 1257-1297.

Liu, B., Mastalerz, M., Schieber, J. SEM petrography of dispersed organic matter in black shales: A review. Earth-Science Reviews, 2022a, 224: 103874.

Liu, B., Wang, Y., Tian, S., et al. Impact of thermal maturity on the diagenesis and porosity of lacustrine oil-prone shales: Insights from natural shale samples with thermal maturation in the oil generation window. International Journal of Coal Geology, 2022b, 261: 104079.

Liu, J., Xie, R., Guo, J., et al. Multicomponent digital core construction and three-dimensional micro-pore structure characterization of shale. Physics of Fluids, 2023b, 35(8): 082003.

Liu, K., Ostadhassan, M., Hackley, P. C., et al. Experimental study on the impact of thermal maturity on shale microstructures using hydrous pyrolysis. Energy & Fuels, 2019, 33(10): 9702-9719.

Liu, K., Ostadhassan, M., Zhou, J., et al. Nanoscale pore structure characterization of the Bakken shale in the USA. Fuel, 2017a, 209: 567-578.

Liu, W., Niu, S., Tang, H. Structural characteristics of pores and fractures during lignite pyrolysis obtained from X-ray computed tomography. Journal of Petroleum Science and Engineering, 2023c, 220: 111150.

Liu, W., Zhang, C., Gao, G., et al. Controlling factors and evolution laws of shale porosity in Longmaxi Formation, Sichuan Basin. Acta Petrolei Sinica, 2017b, 38(2): 175-184. (in Chinese)

Li, X., Jiang, Z., Jiang, S., et al. Synergetic effects of matrix components and diagenetic processes on pore properties in the Lower Cambrian shale in Sichuan Basin, South China. Journal of Natural Gas Science and Engineering, 2021, 94(4-5): 104072.

Löhr, S. C., Baruch, E. T., Hall, P. A., et al. Is organic pore development in gas shales influenced by the primary porosity and structure of thermally immature organic matter? Organic Geochemistry, 2015, 87: 119-132.

Ma, L., Fauchille, A., Ansari, H., et al. Linking multi-scale 3D microstructure to potential enhanced natural gas recovery and subsurface CO_2 storage for Bowland shale, UK. Energy & Environmental Science, 2021, 14(8): 4481-4498.

Mastalerz, M., Schimmelmann, A., Drobniak, A., et al. Porosity of Devonian and Mississippian New Albany Shale across a maturation gradient: Insights from organic petrology, gas adsorption, and mercury intrusion. AAPG Bulletin, 2013, 97(10): 1621-1643.

McGlade, C., Speirs, J., Sorrell, S. Unconventional gas-a review of regional and global resource estimates. Energy, 2013, 55: 571-584.

Medina, C. R., Mastalerz, M., Rupp, J. A., et al. Characterization of porosity and pore-size distribution using multiple analytical tools: Implications for carbonate reservoir characterization in geologic storage of CO_2. Environmental Geosciences, 2017, 24(1): 51-72.

Milliken, K. A compositional classification for grain assemblages in fine-grained sediments and sedimentary rocks. Journal of Sedimentary Research, 2014, 84(12): 1185-1199.

Milliken, K. L., Rudnicki, M., Awwiller, D. N., et al. Organic matter-hosted pore system, Marcellus formation (Devonian), Pennsylvania. AAPG Bulletin, 2013, 97(2): 177-200.

Ohiara, T. M., Taylor, K. G., Dowey, P. J. Mineral diagenesis in a carbonate-rich mudstone: The Lower Carboniferous Hodder Mudstone, UK. Geological Society, London, Special Publications, 2024, 534(1): 201-228.

Ross, D. J. K., Bustin, R. M. The importance of shale composition and pore structure upon gas storage potential of shale gas reservoirs. Marine and Petroleum Geology, 2009, 26(6): 916-927.

Slatt, R. M., O'Brien, N. R. Pore types in the Barnett and Woodford gas shales: Contribution to understanding gas storage and migration pathways in fine-grained rocks. AAPG Bulletin, 2011, 95(12): 2017-2030.

Stasiuk, L. D. Algal bloom episodes and the formation of bituminite and micrinite in hydrocarbon source rocks: Evidence from the Devonian and Mississippian, northern Williston Basin, Canada. International Journal of Coal Geology, 1993, 24(1-4): 195-210.

Sun, M., Fu, J., Wang, Q., et al. Porenetwork characterization and fluid occurrence of shale reservoirs: State-of-the-art and future perspectives. Advances in Geo-Energy Research, 2024, 12(3): 161-167.

Tang, X., Zhang, J., Jin, Z., et al. Experimental investigation of thermal maturation on shale reservoir properties from hydrous pyrolysis of Chang 7 shale, Ordos Basin. Marine and Petroleum Geology, 2015, 64: 165-172.

Taylor, K. G., Macquaker, J. H. S. Diagenetic alterations in a silt- and clay-rich mudstone succession: An example from the Upper Cretaceous Mancos Shale of Utah, USA. Clay Minerals, 2014, 49(2): 213-227.

Theng, B. K. G. Mechanisms of formation of colored clay-organic complexes. A review. Clays and Clay Minerals, 1971, 19: 383-390.

Tian, S., Bowen, L., Liu, B., et al. A method for automatic shale porosity quantification using an Edge-Threshold Automatic Processing (ETAP) technique. Fuel, 2021, 304: 121319.

Tissot, B. P., Welte, D. H. Petroleum Formation and Occurrence (2nd edition). Berlin, Germany, Springer-Verlag, 1984.

Vialle. S., Druhan, J. L., Maher, K. Multi-phase flow simulation of CO_2 leakage through a fractured caprock in response to mitigation strategies. International Journal of Greenhouse Gas Control, 2016, 44: 11-25.

Wang, J., Ryan, D., Anthony, E. J. Reducing the greenhouse gas footprint of shale gas. Energy Policy, 2011, 39(12): 8196-8199.

Wang, J., Wang, K., Shan, X., et al. Potential for CO_2 storage in shale basins in China. International Journal of Greenhouse Gas Control, 2024, 132: 104060.

Wang, L., Liu, B., Bai, L., et al. Maceral evolution of lacustrine shale and its effects on the development of organic pores during low mature to high mature stage: A case study from the Qingshankou Formation in northern Songliao Basin, northeast China. Petroleum Science, 2023, 20(5): 2709-2725.

Wang, L., Zhou, H., Shang, F., et al. Element geochemical characteristics of black shale and paleo-sedimentary environmental restoration of Qingshankou Formation of the Cretaceous in the northern Songliao Basin. Geological Science, 2022, 57(1): 156-171.

Wen, J., Sun, M., Yu, B., et al. Risk assessment of high maturity lacustrine shale oil reservoir based on pore-fracture connectivity and decane accessibility, Ordos Basin (China). Marine and Petroleum Geology, 2024, 168: 107043.

Xiao, D., Zheng, L., Xing, J., et al. Coupling control of organic and inorganic rock components on porosity and pore structure of lacustrine shale with medium maturity: A case study of the Qingshankou Formation in the southern Songliao Basin. Marine and Petroleum Geology, 2024, 164: 106844.

Zhang, C., Wang, Y., Kou, Z., et al. Recent research advancesin enhanced CO_2 mineralization and geologic CO_2 storage. Advances in Geo-Energy Research, 2023a, 10(3): 141-145.

Zhang, S. Diagenesis and mechanism of shale reservoir pore incerase and reduction in Dongying sag. Journal of China University of Mining & Technology, 2018, 47(3): 562-578. (in Chinese)

Zhang, S., Zhang, B., Xiao, M., et al. Gulong shale oil enrichment mechanism and orderly distribution of conventional-unconventional oils in the Cretaceous Qingshankou Formation, Songliao Basin, NE China. Petroleum Exploration and Development, 2023b, 50(5): 1045-1059.

Zhou, J., Liu, B., Shao, M., et al. Lithologic classification of pyroclastic rocks: A case study for the third member of the Huoshiling Formation, Dehui fault depression, Songliao Basin, NE China. Journal of Petroleum Science and Engineering, 2022, 214: 110456.